3 Biotech (2024) 14:227
https://doi.org/10.1007/s13205-024-04058-8

ORIGINAL ARTICLE

Evaluation of cytotoxic potential of silver nanoparticles biosynthesized using essential oils of *Jasminum sambac* against breast cancer and bacterial cells

Ali Kadhum Bidan[1] · **Zainab Shakir Abdullah Al-Ali**[1]

Received: 8 December 2023 / Accepted: 18 August 2024

Abstract
Essential oils (EOs) which cover about 91% whole biomolecules formulated from *Jasminum sambac* leaves based on Gas chromatography-mass spectrometry were employed to identify structures. EOs were observed as good agents in the preparation of Silver nanoparticles (AgNPs) through the proposed mechanism that was attempted to interpret the pathway of the bio-preparation process. The characterization of EOs-AgNPs carried via ultraviolet–visible to reveal surface plasmon resonance at 420 nm, Fourier transform infrared to observe functional groups EOs compared to EOs-AgNPs. X-ray diffraction (XRD) revealed a broad chart owing to the small size of AgNPs in average size less than 10 nm calculated relying on image J software, spherical AgNPs with a small dispersive size observed by transmission electron microscopy. Quasi near spherical surface morphology of EOs-AgNPs had detected by field emission scanning electron microscope. EOs-AgNPs were assessed for their antibacterial potential against both Gram-positive (*Staphylococcus aureus*) and Gram-negative (*Escherichia coli*) bacteria as suppressing bacterial agents. EOs-AgNPs had their anti-breast cancer MCF-7 cell line ability investigated by DNA fragmentation; cycle flow cytometry (apoptosis) at half maximal inhibitory concentration (IC_{50}) was determined at 260 µg/mL which has been stated by cytotoxicity (MTT) assay. EOs-AgNPs have antibacterial and anticancer therapeutic potential, and it is safe, inexpensive, and scalable in the nanoscale range.

Keywords Antibacterial agent · Anti-breast cancer cells · Essential oils · Mechanism biosynthesis of AgNPs · Silver nanoparticles

Introduction

The term "nano" is derived from the Greek word "Nanos," which means dwarf. The nano is a mathematical unit of measurement equal to 10^{-9} m, or one billionth of a meter. Nanomaterials (NM) are a category of substances where at least one dimension is 100 nm or less (Wu et al. 2020). In the present effort to develop new scientific paths, incorporating nanotechnology applications is a potential outcome of integrating applied science and technology in engineering and nano object benefits (Rogers et al. 2007). Nanotechnology inspires nanocomposite synthesis with adjustable properties, and these beneficial bionanomaterials have been widely investigated because of their growing importance in treating disease (Yeh et al. 2012). One of the most famous uses of nanobiotechnology in the medical field is the development of novel antibiotics; simultaneously, nanomaterials play an increasingly crucial role in the emerging field of nanomedicine (Gupta et al. 2019). Bulk materials and nanomaterials have fundamentally various properties; nanostructured materials can be single or multi-phase polycrystals with nanoscale grain sizes and are further classified by dimensions less than 100 nm (Tahir 2018). Nanomaterials based on transition metals are currently attracting a great deal of industrial interest due to their exceptional features, aforementioned characteristics encompass a significantly related area, minimal melting temperatures, distinctive magnetic properties, robust mechanical resistance, and favourable visual capabilities (Verma et al. 2019). It is generally possible to synthesize hetero nanomaterials known as metallic nano species composed of integrating metal into encircling molecules as organic material (Khan 2020). The selection

✉ Ali Kadhum Bidan
ali.bidan.sci@uobasrah.edu.iq

[1] Department of Chemistry, Collage of Science, University of Basrah, Basrah 61001, Iraq

Published online: 10 September 2024

of an appropriate synthesis procedure is vital in producing customized nanoparticles (NPs) since it affects their properties (Kennedy et al. 2014).

Biosynthesis may generate nanoparticles with more precisely defined size and morphology than standard physicochemical production techniques (Azizi et al. 2013). The approach for the large-scale manufacture of nanoparticles is more environmentally friendly, less expensive, and easily scalable compared to conventional chemical and physical procedures (Shankar et al. 2004). Green chemistry is compatible with the production of nanoparticles because the biomolecules produced by the biomass can serve as both reducing and stabilizing agents during the reaction (Bidan and Al-Ali 2024a). For several years, the plant-based synthesis of nanoparticles has garnered substantial interest due to its speed and simplicity (Kalishwaralal et al. 2010). Phenolic compounds such as flavonoids, tannins, and phenolic acids play a crucial role in bioreduction, but they can also serve as capping and stabilizing agents, such as flavanones, which contribute to the surface coating. Proteins and amino acids are covalently bonded to metal nanoparticles (MNPs), capping/coating them to prevent aggregation and stabilizing phyto-MNPs (Selvan et al. 2018).

One BioSource of a biological method with ongoing attention in MNPs synthesis is Essential oils (EOs) (Bidan and Al-Ali 2023) that possess a diverse range of functional groups within their chemical structures, encompassing alcohol, ketone, aldehyde, and lactone groups. These functional groups are characterized by active constituents such as C=C, $–CH_2$, $–CH_3$, –OH, C–H, C=O, C–O–C, $CH_3–C–CH_3$, C–O categories. The presence of active groups in different locations is associated with both reductions and stabilizations, suggesting that these active groups are involved in the precursor of nanoparticles (Sheny et al. 2012). An environmentally safe method for producing biologically nano-silver particles utilizing *Myristica fragrans* essential oil (*M. fragrans*) was described, and liquid oil was employed to convert Ag^+ to nano-silver Ag^0 at 100 °C (Vilas et al. 2014). A recent study has reported an alternative method for the synthesis of silver nanoparticles (AgNPs) using essential oils derived from the leaves of *Coleus aromatics*. This approach is characterized by its simplicity, rapidity, low cost, and environmental friendliness. The synthesis process involves the utilization of a basic solution of sodium hydroxide (NaOH) at a temperature of 100 °C while maintaining an optimal pH (Vilas et al. 2016).

The toxicity of plant latex-encapsulated AgNPs for carcinoma cells was confirmed in human breast cancer cells via DNA damage and the generation of reactive oxygen species (MCF-7 breast cancer cell lines). Researchers discovered that AgNPs are hazardous to breast cancer MCF-7 cells. Green silver nanoparticles (10–30 nm) were synthesized using *Adenium obesum* leaf extract and discovered it induces apoptosis and autophagy (Farah et al. 2016). In another experiment, silver nanoparticles (22 nm) were generated by *Sesbania grandiflora* leaf extract triggering apoptotic cell death in breast cancer cells (Tanaka 1999). The antimicrobial properties of the compounds resulting from the interaction between silver and thiol-containing chemicals are highly potent against a wide range of bacterial strains (Singh et al. 2010). AgNPs are employing *Myristica fragrans* essential oil (*M. fragrans*). Agar well diffusion experiments were used to evaluate synthetic AgNPs against Gram-positive Staphylococcus aureus (*St. aureus*) and Gram-negative Escherichia coli (*E. coli*) bacteria in inhibition zones at 14 mm with 12 mm, respectively (Vilas et al. 2014). *Coleus aromatics* mediated AgNPs synthesis evaluated against *S. aureus* and *E. coli*. This investigation measured the inhibition zone to be gram-positive bacteria 20 mm, and gram-negative bacteria 30 mm (Vilas et al. 2016).

Despite the progress of the biosynthesis of metallic nanoparticles MNPs based on plants, there is an exhibit gap in information that is still form continuous obstacle concerning the lack of understanding of knowing mechanism of green synthesis of MNPs (Guan et al. 2022). The variations observed in the composition of *Jasminum sambac* can be primarily attributed to factors such as the timing of crops, geographic origin, genetic diversity, abiotic factors (including climate, weather, and soil conditions), as well as biotic constraints such as herbivores and parasites (Braun and Sim 2012). The choice of an aqueous precursor solution containing a silver salt for the synthesis of silver nanoparticles is impacted by the varying polarity of essential oils in water, which can potentially restrict the efficiency of the nanoparticle production process (Gao et al. 2017).

The aims of the research attempt to interpret the pathway of mechanism biosynthesis of metal nanoparticles based on EOs-AgNPs, overcome solvent polarity which is concerned with solubility of prepared EOs-AgNPs in distilled water, bioevaluation of EOs-AgNPs investigated compound exhibits notable antibacterial efficacy against both Gram-positive bacteria, specifically *S. aureus*, and Gram-negative bacteria, such as *E. coli*. Additionally, AgNPs demonstrated promising anticancer properties against breast cancer. The MCF-7 cell line is a widely used model in breast cancer research. In else study research also concentrated on using *Jasminum sambac* as a promising reducing and capping agent relying on variant polarity solvents (distilled water) to attract biostructures in synthesis AgNPs (Bidan and Al-Ali 2022), during recent research, relying on various polarity solvent and modifying process of extraction, which resulted to extracting essential oils, therefore replacing solvent in different polarity is necessary to appearing diverse biostructures responsible in creation of metal nanoparticles.

Materials and methods

Chemical materials

The silver nitrate ($AgNO_3$) used in this study was obtained from Alfa Aesar GmbH & Co KG, in Germany. The MTT stain used in this study was obtained from Bio-World in the United States. The antibiotics Ciprofloxacin, Cefuroxime, and Augmentin were sourced from Acino, a pharmaceutical company located in Switzerland. The following reagents were used in the study: fetal bovine serum, RPMI 1640 medium, and Trypsin/EDTA, all sourced from Capricorn (Germany); dimethyl sulfoxide (DMSO), obtained from Santa Cruz Biotechnology (USA); and ethidium bromide (EtBr) and propidium iodide, all acquired from Central Drug House (India). Bacterial species with MCF-7 cultured samples were supplied by Phi Lab Center in Baghdad/Iraq.

Jasminum sambac collection and identification

The collection of fresh leaves of *Jasminum sambac* (L.) Aiton occurred at a blossoming nursery located adjacent to the Tigris River in Baghdad. These leaves were then classified within the Department of Biology, which is part of the Faculty of Science at the University of Basrah in Basrah, Iraq by drawing upon existing scholarly works (Wiersema and Taxonomy 2019). The plant was taxonomically categorized within the Oleaceae family, specifically under the Jasminum genus, and identified as the *Jasminum sambac* species. The leaves of *Jasminum sambac* were excised from the twigs and subjected to a double wash with water to eliminate any dust particles. This was followed by two additional washes with de-ionized water to ensure the absence of impurities. Subsequently, the specimen was permitted to undergo the drying process in a shaded environment, secluded from direct exposure to light, while maintaining ambient room temperature, for a duration of ten days. Subsequently, the desiccated samples were pulverized into fine powders utilizing a household blender. The powder was stored in a sealed container at a temperature of 7 °C until it was ready to be utilized.

Essential oils preparation

A mixture of *Jasminum sambac* leaf powder and absolute ethanol (EtOH) in a 1:10 ratio (%w/v) was subjected to stirring at 350 rpm for a duration of 2 h at a temperature of 50 °C (Bidan and Al-Ali 2023). The resulting solution was allowed to cool and subsequently underwent a double filtration process using a Büchner funnel and Whatman filter paper No.1 under vacuum. The concentrated solution was subjected to rotary evaporation at a temperature of 60 °C to remove any remaining undissolved species. Subsequently, a selected specimen was subjected to thermal treatment within an oven for 2–3 h at a temperature of 60 °C, resulting in desiccation and subsequent storage until required.

Biosynthesis of AgNPs

The experimental procedure for synthesizing silver nanoparticles (AgNPs) involved the utilization of essential oils extracted in (%v/v) a volume ratio of 9:1. A solution containing 0.5 mM $AgNO_3$ was combined with an extracted solution and stirred at (300 rpm) at room temperature for a duration of approximately 3 h to achieve complete bioreduction. This process was characterized by a noticeable colour change from greenish to grey within a time frame of 30 min, as depicted in the graphical abstract (Fig. 1). The EOs-AgNPs were subjected to a colour change process in a sonicator for a duration of 1 h at a power of 120 W. This resulted in the production of finely dispersed EOs-AgNPs. Subsequently, the solution was transferred to a centrifuge and isolated for a period of 25 min at a speed of 7000 rpm. The isolated EOs-AgNPs were then subjected to two rounds of washing with distilled water (DW). Finally, the EOs-AgNPs were subjected to another round of centrifugation for a duration of 15 min to further purify the sample. Ultimately, the EOs-AgNPs should be subjected to a vacuum environment to achieve optimal and desiccated yields.

Characterizations of AgNPs

The process of AgNPs biosynthesis was analyzed using spectroscopic instruments, including ultra-violate–visible (UV–Vis) spectroscopy (Shimadzu UV-1800) and Fourier Transform Infrared Spectroscopy FTIR (IRAffinity-1 Shimadzu) in the range of 400–4000 cm^{-1}. The study of other instruments was conducted using GC–MS (Gas Chromatography-Mass Spectrometry) using a (Varian-Saturn 2200/USA) apparatus. Additionally, X-ray diffraction analysis was performed using a (PHILIPS PW1730) instrument, running at a voltage of 30 kV and a current of 40 mA. The X-ray diffraction utilized Cu Kα radiation with a wavelength of 0.1540 nm. The instrument utilized for transmission electron microscopy (TEM) was the (CM 120 Philips), while selective area electron diffraction (SAED) was measured using the (Tecnai G2 F20). The elemental composition of the silver nanoparticles synthesized using a green synthesis method was analyzed using a combination of field emission scanning electron microscopy (FE-SEM) (MIRA3 TESCAN) coupled instrument of energy dispersive spectroscopy (EDX). The HORIBA SZ-100 instrument was utilized to conduct the dynamic light scattering (DLS) and zeta potential (Z-potential) investigations at a PH level of 6.5.

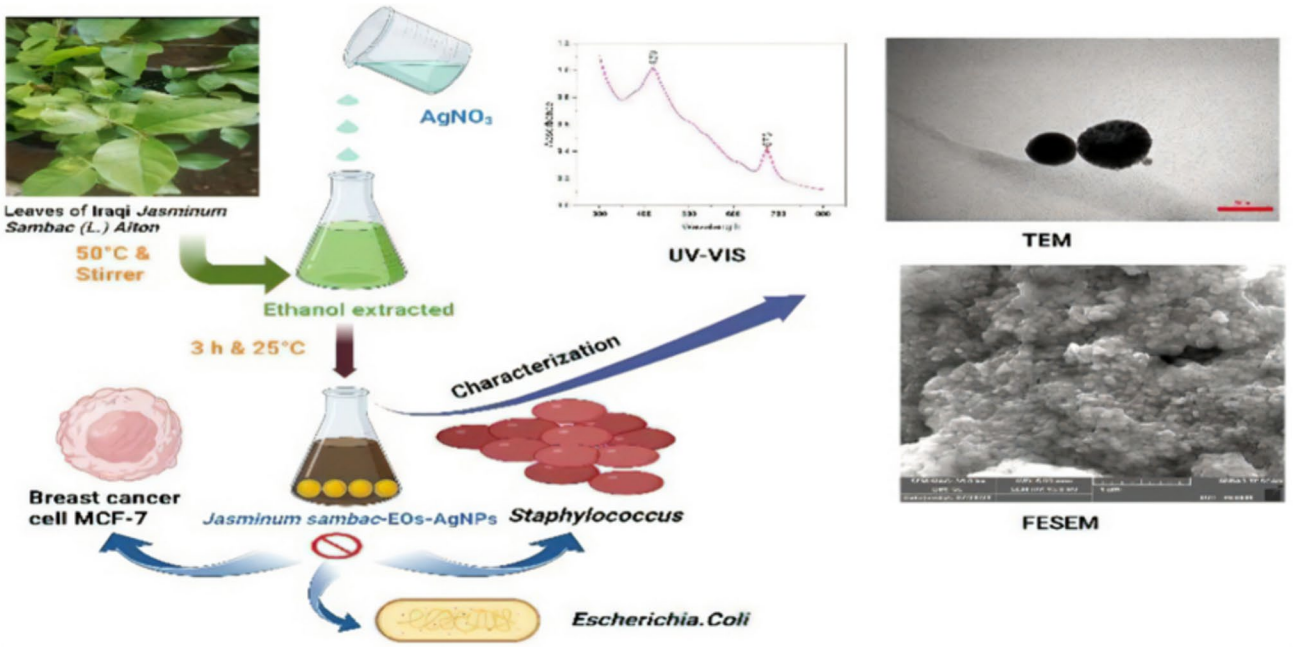

Fig. 1 Biosynthesis of silver nanoparticles (AgNPs) mediated by essential oils (EOs) illustrated its characterization with defeating breast cancer and bacterial cells

Antibacterial activity of AgNPs

This study utilized the disc diffusion method to test the antibacterial activity of EOs-AgNPs, using the agar well diffusion method (Manukumar et al. 2017) against *S. aureus* and *E. coli*. in a preliminary assay with partial modifications. Approximately twenty mL in pure Petri plates, Muller–Hinton (MH) agar was placed aseptically. The bacteria from their stock cultures were captured using a sterile wire loop. Using a sterile tip, 6 mm-diameter wells were drilled into the agar plates after the organisms were cultured. 50µL of EOs-AgNPs were introduced into the pre-drilled holes. Determined levels of EOs-AgNPs in 1000 µg/mL diluted to (500, 250 and 125 µg/mL), another concentration of 500 µg/mL diluted to (250, 125 and 62.5 µg/mL) were presented symbols as (E, B, C, D, respectively and A as control) in images of inhibition zones. Each concentration was tested against both *S. aureus* and *E. coli* and relied on the mean in inhibition zone of (E, B, C, and D) were compared to antibiotic medication such as (Ciprofloxacin, Augmentin, and Cefuroxime). The microorganisms under examination were dissolved in distilled water and subsequently incubated at a temperature of 37 °C for a duration of one night. Following this incubation period, the mean diameter of the region of inhibition was determined. OriginPro 2021 software was used to calculate the mean of inhibition zones in millimetre units (mm).

Cytotoxicity evaluate

Cell viability was assessed through the utilization of an MTT assay, a widely employed method that centers on the reduction of 3-(4, 5-dimethylthiazol-2-yl)-2, 5-diphenyltetrazolium bromide a yellow tetrazolium dye, to a purple-colored water-insoluble formazan within the mitochondria of viable cells. The MCF-7 cells were cultured in RPMI-1640 medium supplemented with 10% Fetal Bovine Serum (FBS), 100 units/mL of penicillin, and 100 µg/mL of streptomycin. The cells were passaged utilizing Trypsin–EDTA, reseeded when they reached 80% confluence twice per week, and subsequently incubated at a temperature of 37 °C. The cytotoxicity of EOs-AgNPs was assessed using the MTT colorimetric assay (Wang et al. 2020). The task was successfully completed with certain modifications. The cell line was cultured in a 96-well plate with a concentration of 4000 cells per well for a duration of 24 h under optimal conditions, which included a temperature of 37 °C, and 5% CO_2 in a humidified incubator. Subsequently, the growth media containing 10% fetal bovine serum (FBS) was aspirated, and the cells were subjected to two rounds of washing using Phosphate buffered saline (PBS). A novel maintenance RPMI medium supplemented with 10% fetal bovine serum (FBS) was utilized in this study. Various concentrations (0.05, 0.5, 5, 50, and 500 µg/mL) of each EOs-AgNPs were introduced to the medium, and the cells were subsequently incubated for a duration of 24 h. The analysis of triple wells was conducted

for every concentration, with the column elution buffer serving as the control. A 10 µL solution of a freshly prepared 0.5 mg per millilitre MTT in phosphate-buffered saline (PBS) was introduced into each well and left to incubate for a duration of 4 h. The media was extracted and replaced with 100 µL of DMSO per well. The plates were subjected to gentle shaking to enhance the solubilization of formazan crystals. The measurement of absorbance was conducted at a wavelength of 545 nm using a microplate reader. The mean optical absorbance of the control group was established at 100%, while the optical absorbance of the remaining investigational groups was determined relative to the control group's value. The cell toxicity percentages and half-maximal inhibitory concentration (IC_{50}) were computed and graphing columns values of cell viability percents based on OriginPro software.

Fracture of DNA measurement

The illustration of single-cell gel electrophoresis (SCGE) by (Singh et al. 1988), involved some modifications, the experiment was carried out with this method to quantify broken DNA strands within individual eukaryotic cells. The cells that are immobilized in agarose on a microscope slide undergo lysis through the use of detergent and high salt. This process results in the formation of nucleoids, which consist of supercoiled loops of DNA that are connected to the nuclear matrix. The application of electrophoresis under alkaline conditions leads to the formation of comet-like structures, which can be visualized using fluorescence microscopy. The relative intensity of the comet tail in comparison to the head is indicative of the extent of DNA fragmentation. The probable rationale behind this phenomenon is that loops that incorporate a break in their structure experience a loss of supercoiling, resulting in their ability to extend towards the anode. The assay possesses various applications, including the evaluation of genotoxicity in newly discovered chemicals, the surveillance of genotoxic environmental contamination, the monitoring of human biomarkers, and the investigation of DNA damage and repair in fundamental research. The MCF-7 cell strain was cultured in 25 cm^2 flasks for a duration of 24 h under controlled conditions of 37 °C and 5% CO_2. Subsequently, the subjects were subjected to treatment with EOs-CuNPs at a concentration equivalent to the half-maximal inhibitory concentration (IC_{50}) for a duration of 48 h, under controlled conditions of 37 °C and 5% CO_2. The cells underwent trypsinization followed by centrifugation at 1000 rpm for 5 min in a new culture medium. Subsequently, they were rinsed twice with ice-cold PBS that was devoid of magnesium and calcium ions, and centrifuged again at 1000 rpm for 5 min. The cells, at a concentration of 1×10^4, were subjected to treatment with agents for a duration of 24 h. Following this treatment, the cells were mixed with low melting point agarose of type VII and subsequently transferred onto a glass slide that had been pre-coated with high melting point agarose of type I. Subsequently, the slides were immersed in a lysis solution containing 2.5 M NaCl, 100 mM EDTA, 10 mM Tris base, and 1% Triton X-100, and adjusted to a pH of 10. The slides were kept at a temperature of 4 °C for a duration of 60 min. Subsequently, the slides underwent a 30-min rinsing process in electrophoresis buffer tris borate EDTA (TBE) at a temperature of 4 °C. In the context of alkaline staining, following the lysis of cells within the solidified agarose medium, DNA was subjected to alkaline treatment with a pH exceeding 13 for a duration of 30 min to induce unwinding. Subsequently, electrophoresis was conducted under the conditions of a voltage of 1.0 V/cm, an intensity of 490 mA, and a duration of 20 min at a temperature of 4 °C. The staining procedure was conducted using the EtBr (0.5 µg/mL) technique. In the present study, the displacement of DNA is utilized as an indicator to quantify the extent of DNA impairment within a specific experimental setting. Following the electrophoresis procedure, the COMET slides were subjected to a washing step using a solution containing 0.4 M Tris–HCl at a pH of 7.5. Subsequently, the slides were fixed for a duration of 10 min using absolute alcohol. A total of one hundred nuclei were enumerated on every slide, and the proportion of cells exhibiting DNA damage and intact DNA was determined. During the enumeration process, the cellular units were classified into two distinct groups: intact DNA and impaired DNA. The DNA damage was documented using a fluorescence microscope (BX53 Olympus, Germany). Based on the size of the tail, the specimens can be categorized into five distinct classes. Class 0 refers to specimens with no tail, while class 1 includes specimens with tails that are shorter than the diameter of the head (nucleus). Class 2 comprises specimens with tail lengths ranging from 1 to 2 times the diameter of the head. Specimens falling under class 3 possess tails that are more than twice the diameter of the head. Finally, class 4 encompasses specimens that lack a head and exhibit severe damage.

Cell cycle arresting investigation

Cell cycle arrest was induced in MCF-7 cells by seeding them in 12-well plates using a standard growth medium at a density of 1×10^5 cells per well. Subsequently, the cells were permitted to adhere for a duration of 24 h, following which the medium was substituted with an exposure medium for a period of 72 h. Subsequently, the exposure medium was replenished based on the IC_{50} value of EOs-AgNPs. Following a 24 h incubation period, the cells were collected and subsequently rinsed with phosphate-buffered saline (PBS). The cell pellets were subjected to staining using a 1 mL solution of propidium iodide (PI) stain, which was

prepared freshly. The staining solution consisted of 0.1% Triton X-100, 0.1% sodium citrate, 50 g/mL PI, and 10 g/mL of RNase A dissolved in phosphate-buffered saline (PBS). Cells can be stored for a duration of 1 h up to overnight in a dark environment at a temperature of 4 °C before conducting flow cytometry analysis. Fluorescence spectrophotometry (CyFlow, Partec Co., Germany) was employed to conduct flow cytometry measurements. Following linear amplification, the collection of PI fluorescence was conducted using a bandpass filter with a wavelength range of 575/25 nm, specifically targeting orange-red fluorescence (FL2). The proliferative capacity of a chemical substance in a flow cytometry assay is determined by observing the alteration in the percentage of cells within different phases of the cell cycle. The relative proliferative effect percentage (RPE%) is determined by calculating the percentage of cells in the S-phase of EOs-AgNPs-treated samples compared to the negative control.

Result and discussion

Surface plasmon resonance (SPR) determination

The determination of AgNPs synthesis has been established through the observation of a colour transition from green to greyish, which signifies the occurrence of Local Surface Plasmon Resonance (LSPR) phenomena. The characterization of EOs-AgNPs generated using essential oils was conducted using UV–Vis spectroscopy, which revealed a prominent absorption peak (λ_{max}) at 420 nm (Fig. 2), with appearing small another peak at 675 nm due to presenting functional groups that possess π orbitals; when subjected to UV–Vis radiation, these groups will undergo exciting transitions at the π–π^* level, in present water as a solvent with remains of polar absolute ethanol mean rising polarity leading to diminishing energy gap occurring red shift wavelength available between 630 and 670 nm followed bioreduction ion process of silver ions Ag^+ to silver nanoparticle Ag^0. LSPR is a technique that generates coherent

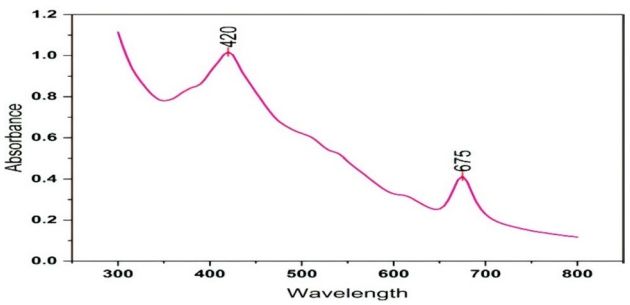

Fig. 2 Ultraviolet–Visible (UV–Vis) spectrum of determined EOs-AgNPs surface plasmon resonance in greatest absorption

electron oscillations by interacting electromagnetic radiation with nanoparticles of metal (Ammari et al. 2016). UV–Vis spectroscopy and colour reaction were used to detect silver nanoparticles between 400 and 500 nm (Lava et al. 2021).

Functional groups of EOs analysis in FTIR

The observed peaks at wavenumbers 3282, and 2924 cm^{-1} (Alharbi et al. 2023) along with 1708 cm^{-1} may be attributed to the stretching vibrations of O–H, aliphatic C–H, and C=O bonds in flavonoids and phenolic groups. The peak observed at 1450 cm^{-1} is indicative of the polyphenol hydroxyl (OH) group, providing evidence for the existence of an aromatic moiety. Additionally, the absorption peaks detected at 1068 cm^{-1} have been attributed to the presence of the carbon–oxygen (C–O) functional group in Fig. 3A. While was observed change in the nature of biofunctional group peaks location was attributed to the form of silver nanoparticles AgNPs, by the way, shifting in peaks at 3464 cm^{-1} OH group bounded, 2916 cm^{-1} aliphatic C–H, 1705 cm^{-1} of C=O stretching vibration, and 1041 cm^{-1} were assigned for C–O group (Fig. 3B) (Pretsch et al. 2020). The variations between the FTIR spectra of the extracted plant and the plant extract based on AgNPs indicate the chelation formation of the Ag ions and the –OH functional groups (Morales-Lozoya et al. 2021). Consequently, minor variations in the transmittance percent of AgNPs spectra may be attributable to the binding of bioactive substances to metal surfaces (Nguyen et al. 2020). These distinct peaks support the existence of polyphenolic chemicals in the extract, which may act as a bioreduction in the synthesis of AgNPs via silver nitrate reduction (Dua et al. 2023).

Structures identification of essential oils

The solution that was extracted was subsequently analyzed using gas chromatography-mass spectrometry (GC–MS) with the Varian-Saturn 2200 instrument (United States). GC–MS mother chart was investigated with 13 structures extracted with 100% ethanol. Almost all constituent substances extracted from leaves were essential oils, which comprised 91% of Oleic acid with one derivative, Palmitic acid with two derivatives, and two linoleic acid derivatives, which play the majority roles in the bioreduction of Ag^+ ions to Ag^0 nanoparticles. Besides that, 2.49% of 5-hydroxymethylfurfural participated in capping AgNPs created by essential oils. Another structure in GC–MS, in which cooperation in stabilization formed AgNPs, was Propylene glycol, Phytol, and Elaidolinoleyl alcohol, and 5-Hydroxymethylfurfural which it forges the remaining extracted solution, as shown in Fig. 4. The existence of phytochemical compounds was determined by measuring retention time, mass spectra, and a chemical library. The chemical compounds that have

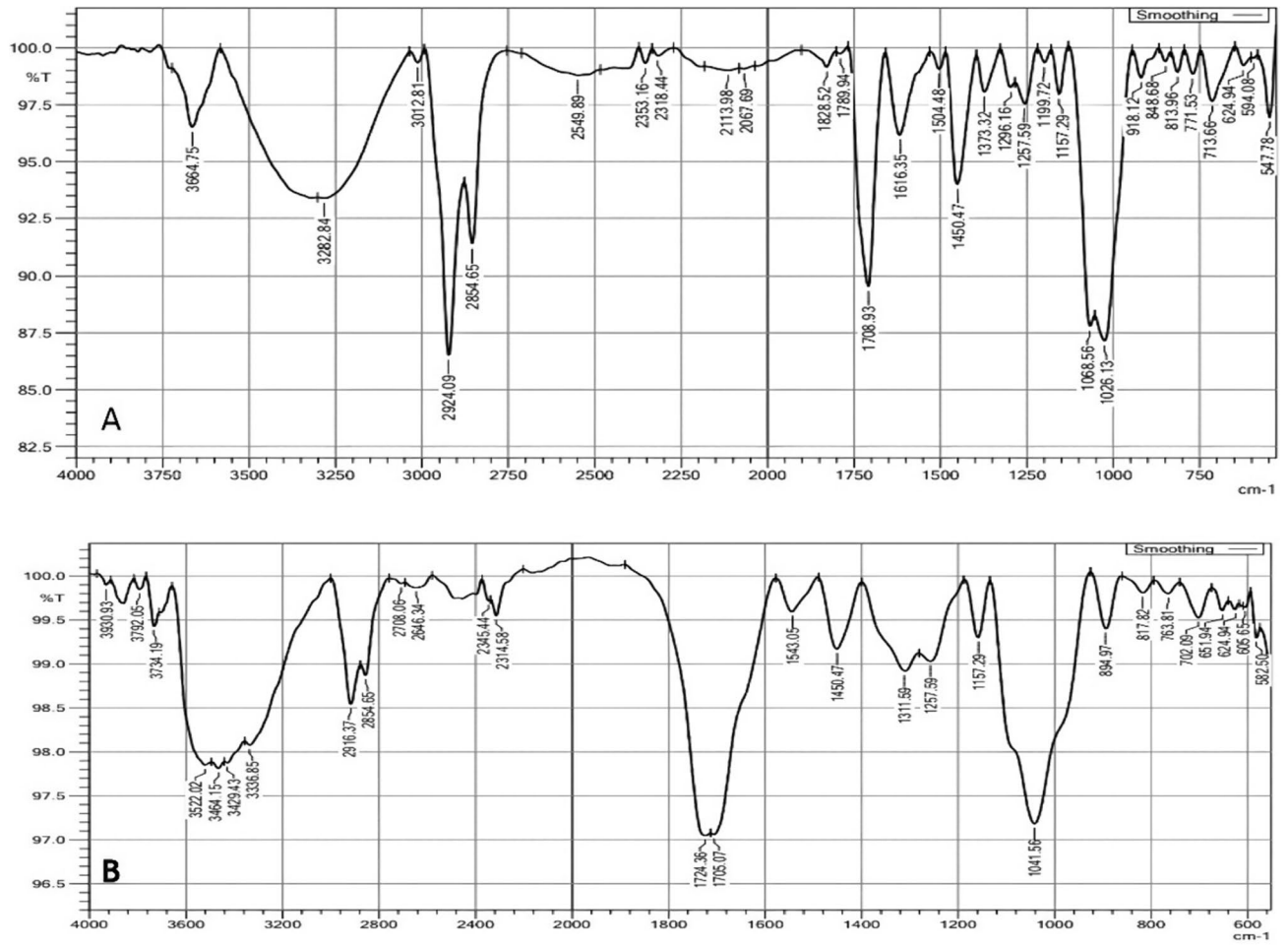

Fig. 3 **A** Fourier transform infrared spectroscopy (FTIR) of essential oils extracted from *Jasminum sambac* leaves, **B** EOs-AgNPs after the bioreduction process

been identified, along with their corresponding molecular structures, are presented in Table 1. The National Institute of Standards and Technology (NIST) and Wiley computer library were employed to ascertain the identification of substances through the application of probability-based matching techniques.

Significant essential oils as biocompounds connected with the suggested synthesis mechanism in this study (Fig. 5) were found in GCMS analysis spectra dependent on three stages of major biological activities. (i) During the activation stage, reduction and nucleation of metal ions occur facilitated by active secondary metabolites. (ii) The combination of adjacent nanomaterials leads to the formation of larger particles, thereby enhancing the thermodynamic stability of the nanomaterials through the utilization of hydrogen bonds. (iii) The production of nanomaterials takes place at the final level (Ali et al. 2021; Si and Mandal 2007). During the activation step, the electrostatic interaction between metal ions and functional groups found in the structure of metabolites, such as carbonyl and hydroxyl groups, is a significant phenomenon resulting in the reduction process of AgNPs (Naseer et al. 2020). According to the mechanism, functional groups are converted into a carbonyl group following their reduced state (polyphenols). Produced reducing metal ions by reduction processes, resulting in an oxidized form of polyphenols as carbonyl groups leading to AgNPs are stabilized by electrostatic attraction.

The transmission electron microscopy image (Fig. 6) verifies the proposed process explanation for the formation of spherical AgNPs after reduction and capping. The image demonstrates how attaching (capping) phytochemical groups to AgNPs resulted in a stabilized overall configuration. The size, morphology, and quality of the synthesized nanoparticles (NPs) are influenced by various factors, such as the concentration of metal salt, plant extract, pH of the solution, reaction time, and temperature (Karimi and Mohsenzadeh 2015).

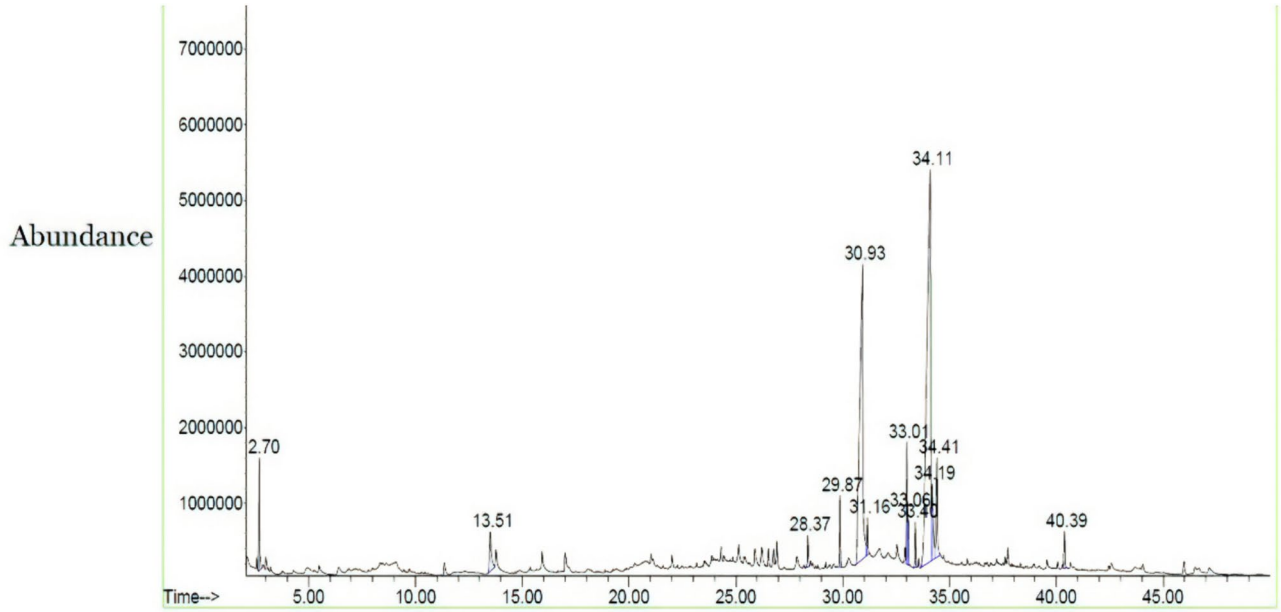

Fig. 4 Gas chromatography-mass spectrometry (GC/MS) chromatogram of essential oils (EOs) structures identification

X-ray diffraction determination

XRD is a technique for measuring the angles and intensities of X-ray beams that are diffracted. Depending on the X-ray's incident wavelength (Bunaciu et al. 2015), the amplification of wave amplitude can occur as a result of constructive interference that is noticed within the evaluation. Commonly used for determining silver nano's crystalline structure (Agnihotri et al. 2014), the XRD method is widely employed. Analyzed peaks at 37.49, 44.27, 64.77, and 77.08 as appeared in Fig. 7. The crystal structures of the samples were determined to be face-centered cubic (FCC) with Miller indices of (111), (200), (220), and (311), respectively. This analysis was conducted using X'Pert HighScore software, and the standard JCPDS card No. 00-004-0783 was used as a reference. The X-ray diffraction (XRD) technique used to determine the size of nanoparticles is based on the observation that as the size of particles decreases, the XRD patterns exhibit increased diffuseness. The diminishment of signal strength and the overlapping of peaks pose challenges in distinguishing between nanoparticles smaller than 10 nm due to the phenomenon of peak broadening (Bidan and Al-Ali 2024b). This condition hindered the process of estimating the size of nanoparticles and characterizing crystals (Holder and Schaak 2019).

To elucidate the crystalline phases of the AgNPs, a meticulous examination of selective area electron diffraction (SAED) represents an additional approach for the analysis of materials, facilitating the investigation of their crystalline architecture. One notable advantage of this technique is its compatibility with electron microscopy investigations. The analysis may be conducted on a designated sample region, enabling the acquisition of data regarding the crystalline structure of distinct components within composite materials, particularly for individual nanoparticles. Nevertheless, the identification of inorganic crystal compounds can be achieved through the analysis of distinct angles obtained from X-ray diffraction (XRD) measurements. On the other hand, selected area electron diffraction (SAED) offers valuable insights into the fundamental properties of the crystal structure (Pryshchepa et al. 2020). As shown in Fig. 8 when applying SAED's interplanar distance measuring technique of (0.239, 0.204, 0.1439, and 0.123) well-matching silver nano FCC as (0.235, 0.204, 0.144 and 0.123) (Boutinguiza et al. 2015), depending on FCC principle, there are four atoms in the FCC per unit cell structure.

Transmission electron microscopy (TEM) imaging

TEM images of nanomaterials created with an electron beam. This technique is used to determine the size and appearance of nanomaterials. TEM can also be used to determine the size distribution of nanomaterials (Bhavyasree and Xavier 2021). The defined shape of EOs-AgNPs looking tiny spherical particles attached to hazy areas corresponded to biomolecules enforced bioreduction (Landeros-Páramo et al. 2022) shown in Fig. 9A. Size distribution countered by Image J software determined the particle size to be an average at 5.8 nm been appeared in Fig. 9B.

Table 1 GC/MS investigation for identified structures of essential oils

No	Retention time (min)	Area of peak %	Identified compounds	Molecular formula	Molecular weight (g/mol)	Chemical structure
1	2.69	2.51	Propylene glycol	$C_3H_8O_2$	76.09	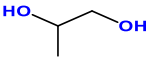
2	13.50	2.49	5-Hydroxymethylfurfural	$C_6H_6O_3$	126.11	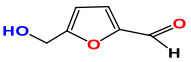
3	28.37	0.96	1,2-Benzenedicarboxylic acid, butyl 2-methyl propyl ester (Butyl isobutyl phthalate)	$C_{16}H_{22}O_4$	278.34	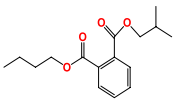
4	29.87	1.77	Hexadecanoic acid, methyl ester (Methyl palmitate)	$C_{17}H_{34}O_2$	270	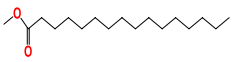
5	30.93	29.71	Hexadecanoic acid (Palmitic acid)	$C_{16}H_{32}O_2$	256.42	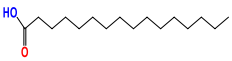
6	31.16	1.10	Hexadecanoic acid, ethyl ester (Ethyl palmitate)	$C_{18}H_{36}O2$	284.5	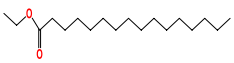
7	33.01	3.32	9,12,15-Octadecatrienoic acid, methyl ester (α-Methyl linolenate)	$C_{19}H_{32}O_2$	292.5	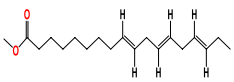
8	33.06	1.17	9-Octadecenoic acid, methyl ester (Oleic acid methyl ester)	$C_{19}H_{36}O_2$	296.5	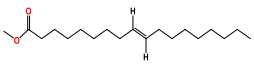
9	33.40	1.15	Phytol	$C_{20}H_{40}O$	296.5	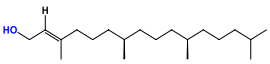
10	34.11	46.95	9-Octadecenoic acid (Oleic acid)	$C_{18}H_{34}O_2$	282.5	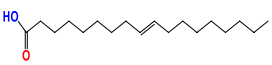
11	34.19	3.68	9,12,15-Octadecatrienoic acid, ethyl ester (Ethyl linolenate)	$C_{20}H_{34}O_2$	306.5	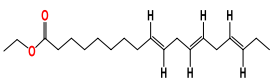
12	34.41	4.00	Octadecanoic acid (Stearic acid)	$C_{18}H_{36}O_2$	284.5	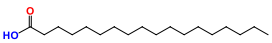
13	40.39	1.18	9,12-Octadecadien-1-ol (Elaidolinoleyl alcohol)	$C_{18}H_{34}O$	266.5	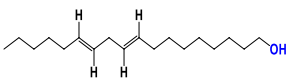

FESEM and energy dispersive X-ray (EDX) examination

Field emission scanning electronic microscopy (FESEM) is another type of microscope that utilizes focused electron beams to scan nanomaterial surfaces. This approach provides signals that contain information on the sample's surface topography. It is utilized for imaging at a higher magnification. The surface morphology was significantly affected by the plant leaf extract used as a reducing and capping agent, according to FESEM data. They were shown in spherical geometry to characterize the surface morphology of the EOs-AgNPs (Fig. 10A). Energy dispersive X-ray (EDX) determines nanomaterials' qualitative and quantitative elemental composition (Bhavyasree and Xavier 2021). Ag, C, O, and Cl peaks are observed during the production of silver nanoparticles by attaching them to essential oils. Calculated percentages of Silver, carbon, oxygen, and chlorine produced from EOs-AgNPs leaves are 41.7, 34.4, 11.9, and 11.9%, respectively, clarified in Fig. 10B.

Dynamic light scattering (DLS) and Z-potential measurement

DLS is a method to calculate particle size; measurements take a few minutes, and the instrument is reasonably priced (Lee et al. 2016). The hydrodynamic radius, described as a hypothetical hard sphere diffusing, affects DLS (Bhattacharjee 2016). The size of a DLS differs from the size of a TEM. DLS measurements of EOs-AgNPs are often greater than those of XRD and TEM due to the statutes; DLS readings are affected by metal configuration, encapsulating, as well stabilizing chemicals which gather on NPs' surfaces (Alsharif et al. 2020). Synthesized silver nanoparticles based on essential oils have an average size of 214.9 nm. The size distribution of the particles is

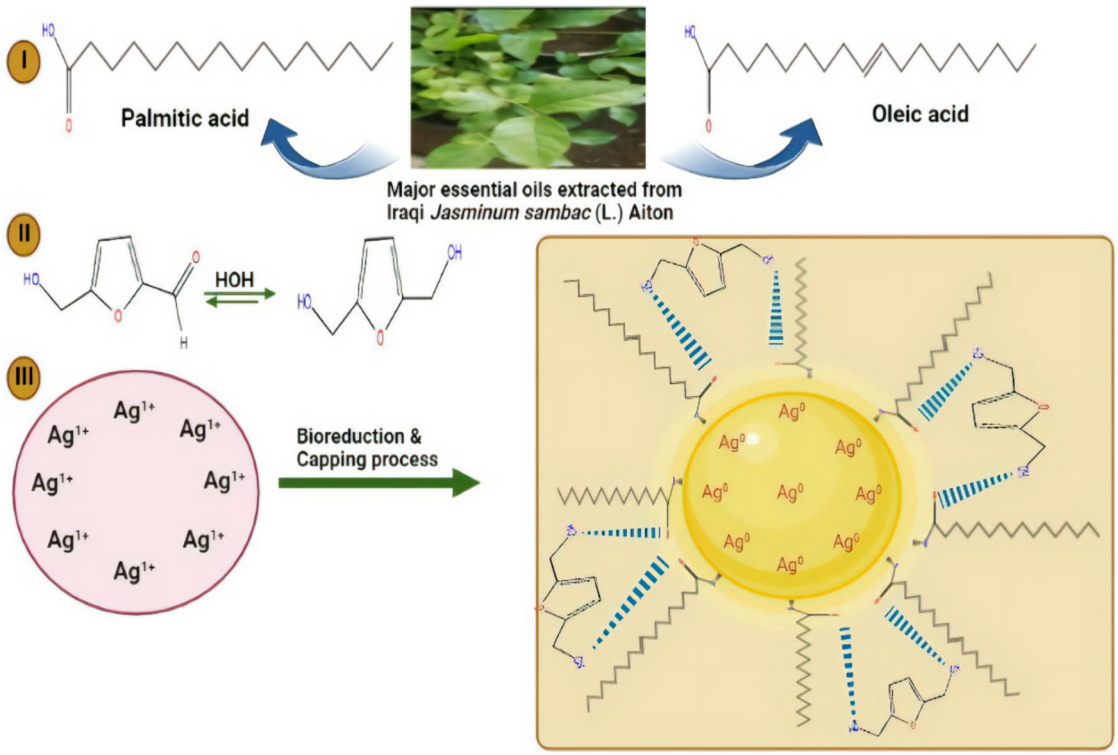

Fig. 5 Proposed mechanism steps biosynthesis of silver nanoparticles (AgNPs) in the presence of essential oils as reducing and capping agents

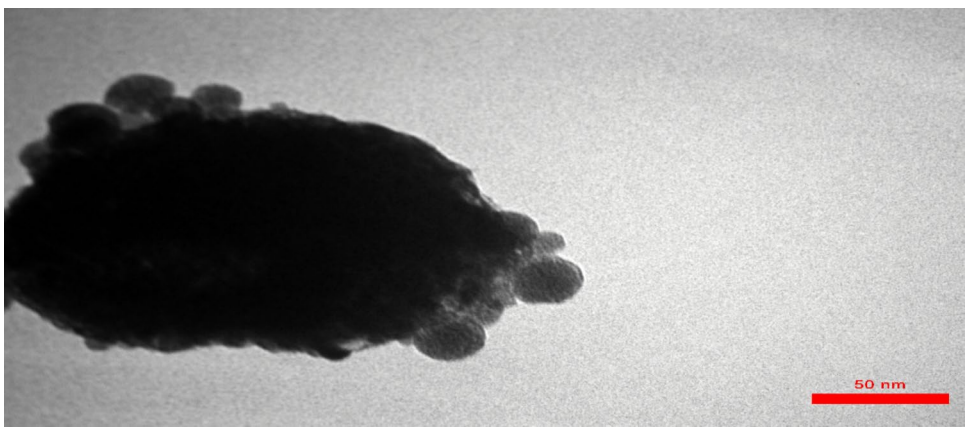

Fig. 6 Transmission electron microscopy (TEM) showing the capping of reduced AgNPs by essential oils in the nanoscale range

uniform, and the polydispersity index is 0.388 (Fig. 11A). The nanomaterials' stability and surface charge density were assessed using zeta potential analysis (Bhavyasree and Xavier 2021). Z-potential study reveals that Nanoparticles in a colloidal form are stable. This can be inferred that stable colloidal nanoparticles necessitate a Z-potential exceeding +30 mV or falling below −30 mV (Balasubramanian et al. 2020). The surface silver nanoparticles exhibited a Z-potential value of −18 mV upon synthesis of EOs-AgNPs (Fig. 11B).

Bacterial suppressing ability of EOs-AgNPs

Bacteria have grown to prominence among microorganisms due to their inherent biological characteristics, such as their manageability, fast proliferation, and genetic adaptability (Tshikantwa et al. 2018; Amenah and Al-Ali 2024). The antibacterial efficacy of silver nanoparticles synthesized through an environmentally friendly approach was successfully demonstrated against bacterial including *S. aureus* along with *E. coli* (Princy et al. 2023; Al-Majeed

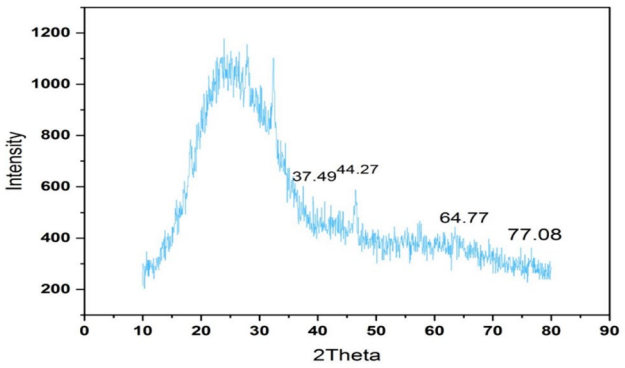

Fig. 7 X-ray diffraction (XRD) diffraction analysis of EOs –AgNPs exhibited a broad pattern in a small nanoscale

et al. 2023) as illustrated in Fig. 12 when compared with classical antibiotic drugs as appeared in Figs. 13, 14 were observed all agents used have ability to destroying bacterial species; in detailing data scheduled based mean of suppressing zone were showed low mean concentrations of AgNPs were inhibited *S. aureus* beside *E. coli* more than high mean concentrations, in addition to all mentioned, AgNPs were considered to have a higher ability in defeating bacterial colonies than antibiotic medications as appeared in Table 2. AgNPs at a low concentration of 500 µg/mL appear more actively opposite in both *S. aureus* and *E. coli* than at a high concentration of 1000 µg/mL, Owing to the large surface area of AgNPs, they gave enhanced contact with microorganisms (Logeswari et al. 2015). Using agar well diffusion assays, Gram-positive *S. aureus* and Gram-negative *E. coli* bacteria were used to assess AgNPs synthesized with the essential oil of *Myristica fragrans*. *E. coli* and *S. aureus* at 100 mg/mL 14 and 12 mm, respectively, exhibited the most significant zone of inhibition (Vilas et al. 2014). According to *Coleus aromatics*-essential oils, promoted the synthesis of AgNPs and their antibacterial activity against *S. aureus* and *E. coli*. In this investigation, the inhibition zone was 20 mm for Gram-positive bacteria and 30 mm for Gram-negative bacteria, respectively (Vilas et al. 2016). The nature of the relationship between Gram-negative with proposed MNPs as antibacterial noted by way of the decreased response of negative microorganism sort (*E. coli*) to the existence of nanostructures is able to demonstrate through the presence

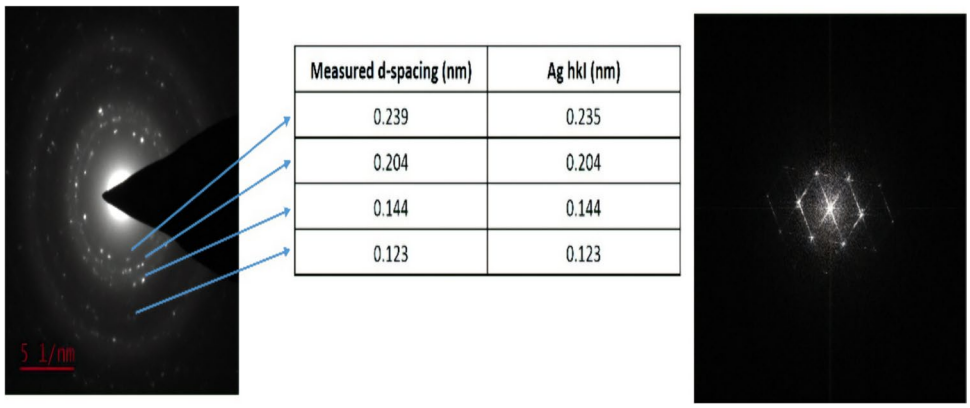

Fig. 8 Selective area electron diffraction (SAED) of prepared silver nanoparticles revealing crystallography configuration status

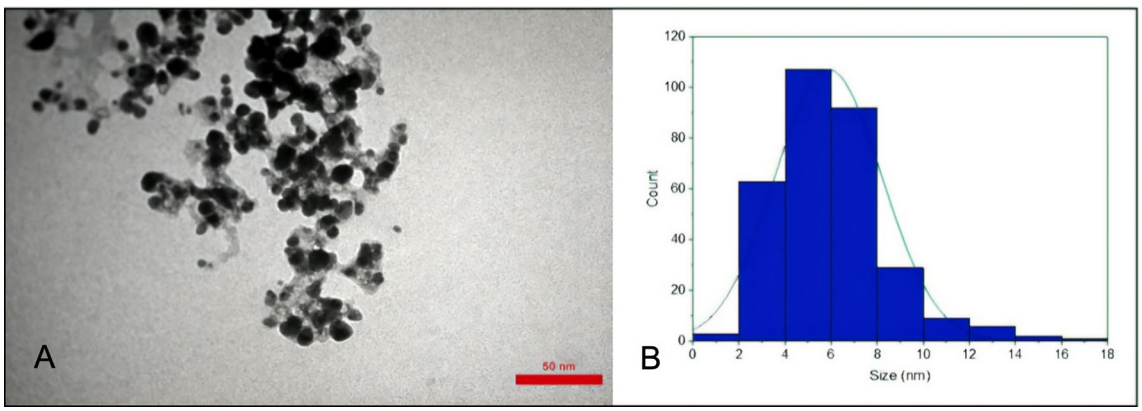

Fig. 9 **A** Silver nanoparticles created based on essential oils depict a set of nanoparticles in TEM imaging. **B** The size distribution and average diameter of EOs-AgNPs are shown by image J software

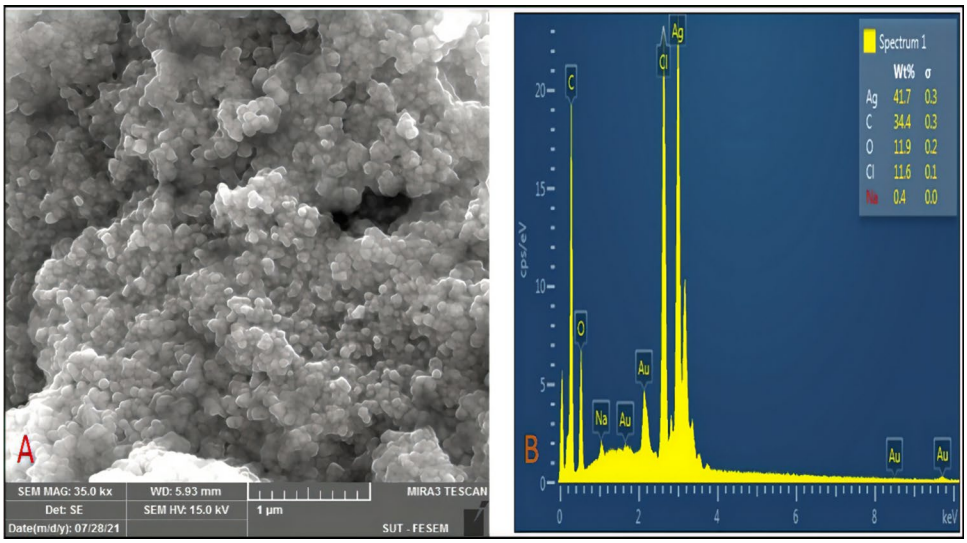

Fig. 10 **A** Field emission scanning electron microscopy (FE-SEM) exhibited surface morphology of EOs-AgNPs. **B** Elemental nanocomposition included in EOs-AgNPs by energy dispersive X-ray (EDX)

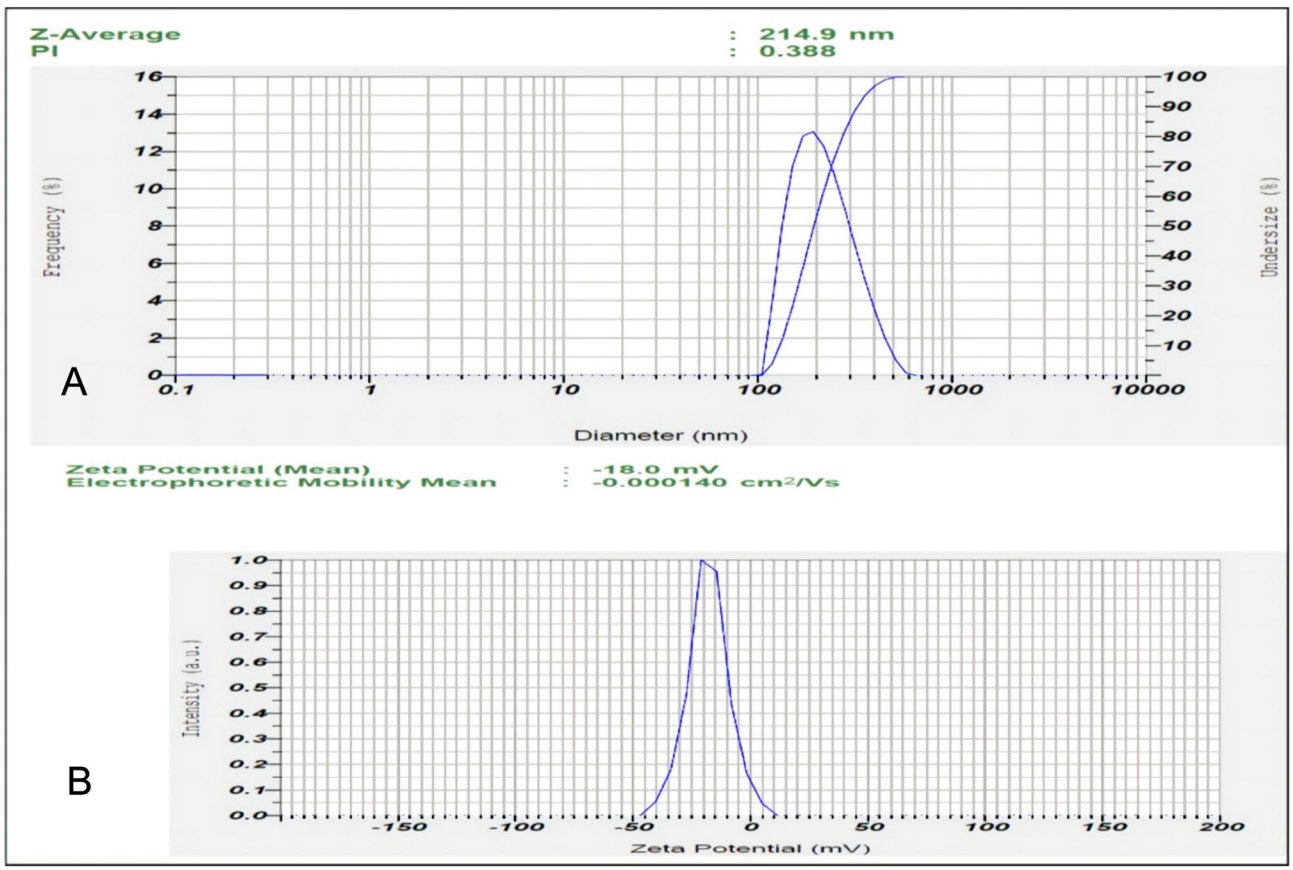

Fig. 11 **A** Dynamic light scattering (DLS) analyzing the graph of hydrodynamic radius for EOs-AgNPs. **B** Z-potential analysis to appearing charge stability of EOs-AgNPs

of lipopolysaccharide (LPS) upper portion of their tissue, which restricts the spread of constituents (Maciel et al. 2020). In published results, biomolecule essential oils utilized as reducing agents in the production of AgNPs were found to have enhanced powers against bacterial colonies, particularly Gram-negative *E. coli*, and diminished their resistance potential.

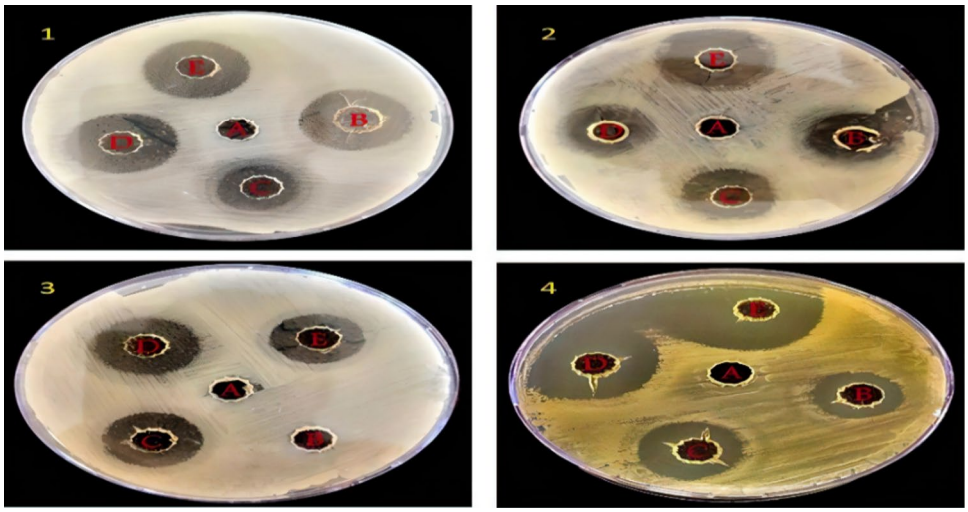

Fig. 12 Biosynthesized of EOs-AgNPs showed defeating activity against *S. aureus* (**1**, **2**), and against *E. coli* (**3**, **4**) at 1 and 0.5 mg/mL, respectively

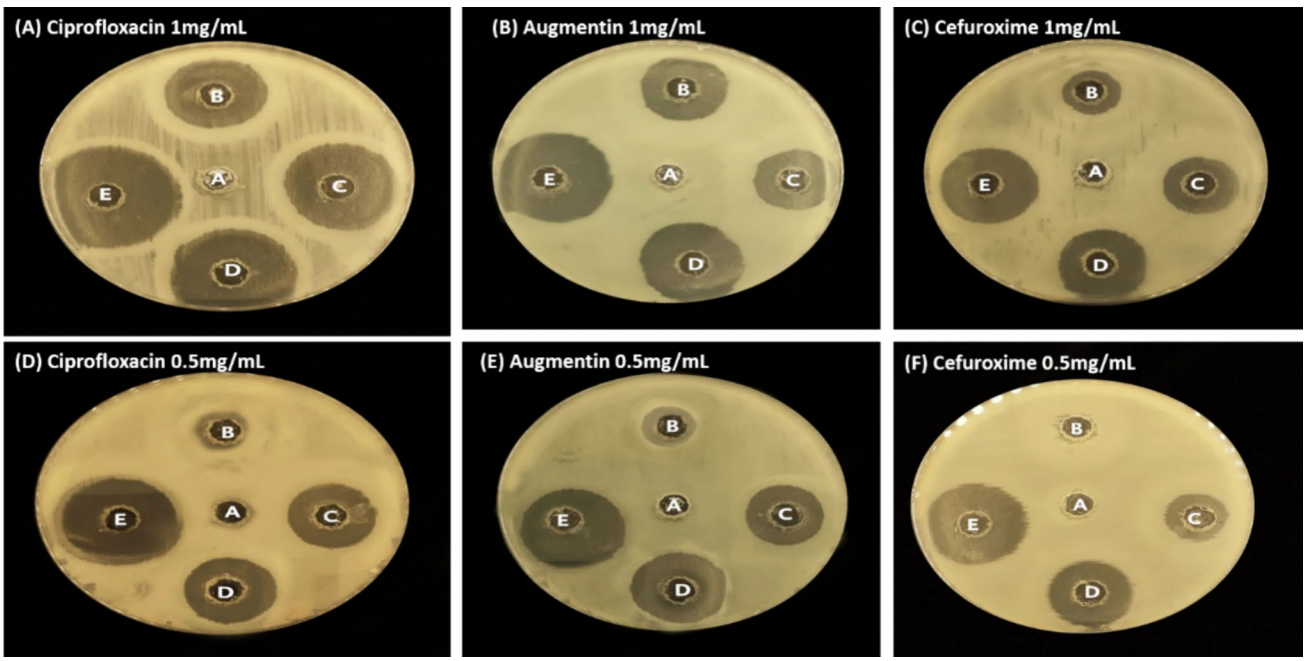

Fig. 13 Antibacterial activity of antibiotic medications (Ciproflaxaci, Augmentin, and Cefroxime) against *S. aureus*

Cell viability investigation of EOs-AgNPs

The dose-dependent effect of EOs-AgNPs produced nano-conjugates on MCF-7 cells was a decrease in cell viability and an increase in inhibition rate. The observed cell viability percentage decreased from 94.66 to 29.61% between (0.05, 0.5, 5, 50, and 500 µg/mL), indicating a dose-dependent impact of AgNPs. This experiment was utilized in the account of IC_{50}, as shown in Fig. 15.

The surface-attached cells proliferated at a 96–100% rate. MCF-7 cells dealt in EOs-silver nanoparticles exhibited cellular apoptosis. The once-reported study, signed to production conducted in this study primarily centered on the ethanolic extract of *Jasminum sambac* created nano's silver which arrested MCF-7 cells (El-Hawary et al. 2019) at 1 mmol $AgNO_3$ and identified different phytochemical structures extracted did not signal to EOs, in present experiment IC_{50} of EOs-AgNPs at 260 µg/mL detected after 24 h. The treatment of AgNPs with ultrasonic waves revealed an additional effect in lowering MCF-7 cell viability. Induction using Ultrasound Accumulation of reactive oxygen species (ROS) in cells can be triggered by cavitation. Subsequently, cellular ROS buildup sets off a cascade of actions. Cavitation's reactive oxygen species were harmful to DNA and

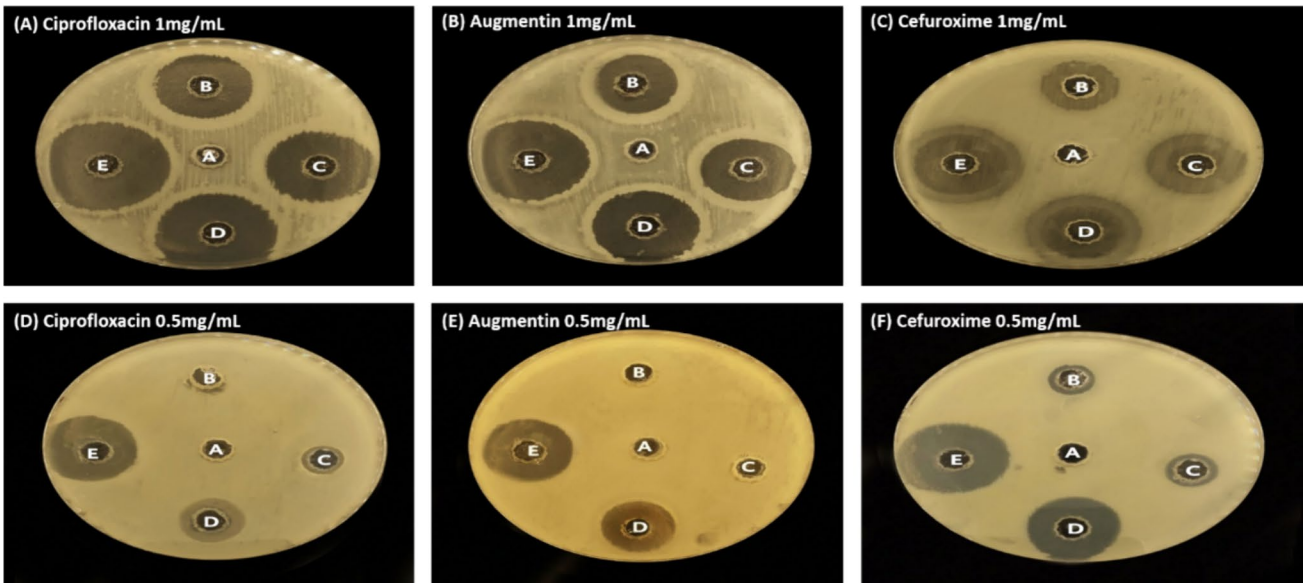

Fig. 14 Antibacterial activity antibiotic medications of (Ciprofloxacin, Augmentin, and Cefroxime) against *E.coli*

Table 2 Data of antibacterial activity comparison between EOs-AgNPs with some antibiotic drugs

Name of antibacterial	Concentration (mg/mL)	Bacteria	Mean of inhibition zone (mm)
EOs-AgNPs (1)	1	*Staphylococcus aureus*	29.25
EOs-AgNPs (2)	0.5	*Staphylococcus aureus*	35.25
EOs-AgNPs (3)	1	*Escherichia coli*	24.75
EOs-AgNPs (4)	0.5	*Escherichia coli*	39.5
Ciprofloxacin	1	*Staphylococcus aureus*	24
Augmentin	1	*Staphylococcus aureus*	19
Cefuroxime	1	*Staphylococcus aureus*	18
Ciprofloxacin	0.5	*Staphylococcus aureus*	20
Augmentin	0.5	*Staphylococcus aureus*	19
Cefuroxime	0.5	*Staphylococcus aureus*	17
Ciprofloxacin	1	*Escherichia coli*	24
Augmentin	1	*Escherichia coli*	23
Cefuroxime	1	*Escherichia coli*	18
Ciprofloxacin	0.5	*Escherichia coli*	17
Augmentin	0.5	*Escherichia coli*	16
Cefuroxime	0.5	*Escherichia coli*	18

interfered with mitochondrial activity (He et al. 2015). Effect biosynthesized AgNPs from Ag source at 1 mmol or greater in high linked to another reactant extracted solution led to enhancing AgNPs IC_{50} against breast cancer cell line MCF-7 values such as employing 99 mL of Ag source to 1 mL of extracted plant dissolved in aqueous media (Al-kawmani et al. 2020). In a prior work utilizing a crude ethanolic extract of *O. arabicus* in the creation AgNPs, the IC_{50} concentration in MCF-7 cells was determined to be 562 µg/mL (Ali et al. 2016). Under inverted microscopy, the morphology of MCF-7 cells treated with EOs-synthesized AgNPs for 24 h was studied. Control cells had a typical shape. MCF-7 cells treated with EOs-synthesized AgNPs exhibited obvious cell death. In addition, a loss of cell adhesion, a reduction in cell size, and a fall in cell density all contributed to the shrinkage of cells (Fig. 16). When evaluating the cytotoxicity of nanoparticles, it is essential to take into account various factors such as their shape, size, composition, surface hydrophobicity, and surface charge (Fröhlich 2012).

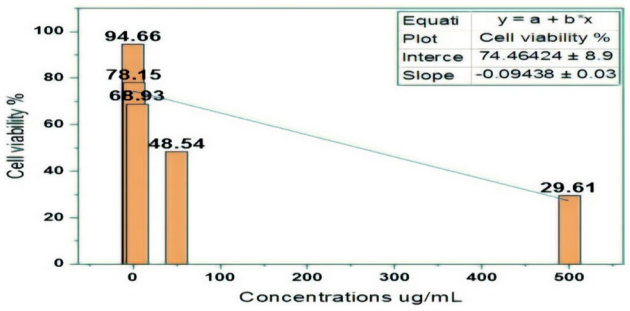

Fig. 15 Antiproliferation efficacy of EOs-AgNPs versus the MCF-7 cell type as Half-maximal inhibitory concentration (IC_{50}) at 260 µg/mL

Comet assay fragmentation of EOs-AgNPs

The capacity of EOs-AgNPs to cause genetic damage in MCF-7 cells. The results demonstrate genetic damage (as measured by tail remaining) at IC_{50} concentration of EOs-AgNPs, which were considerably genotoxic to MCF-7 cells as indicated by concentration-dependent proportionate increases in DNA fragmentation. Images under a microscope demonstrated that handled nuclei had lengthier comet tails considerably matching the destroyed head of treated cells (C, F) compared to control (untreated cells) cells (A, D) exhibited a whole cell structure (Fig. 17). Synthesized AgNPs cause DNA damage in MCF-7 cells. An important feature of DNA damage is the creation of free radicals (oxidative stress), which predominantly affects single-strand break and olive tail movement resulting in tissue collapse (Piao et al. 2011). Silver nanostructures suppress the growth of human

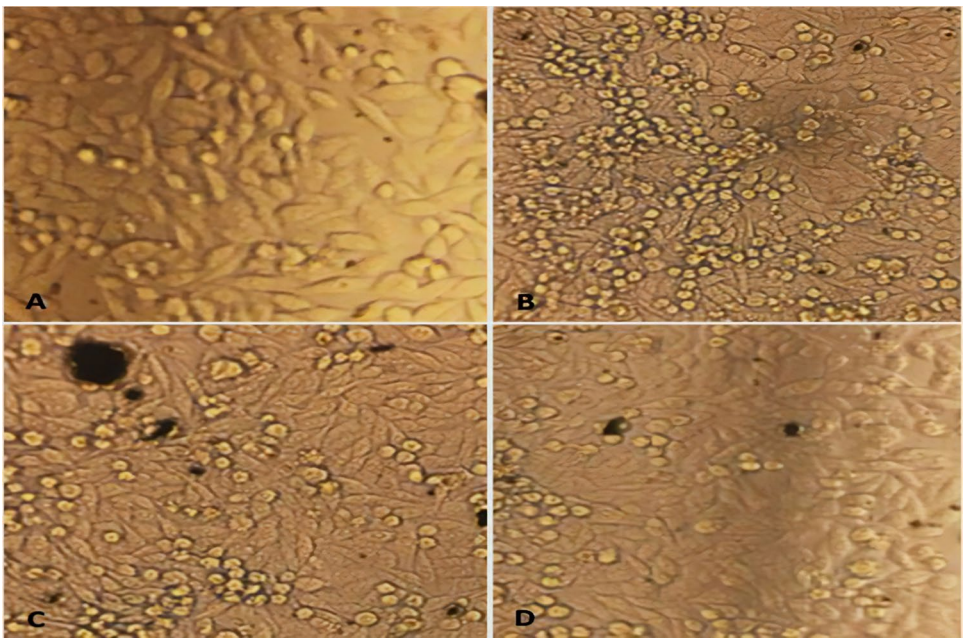

Fig. 16 **A** Microscopic images of untreated MCF-7 breast cancer cells, **B**–**D** images of treated MCF-7 cells by EOs-AgNPs at (500B-50C-5D at µg/mL)

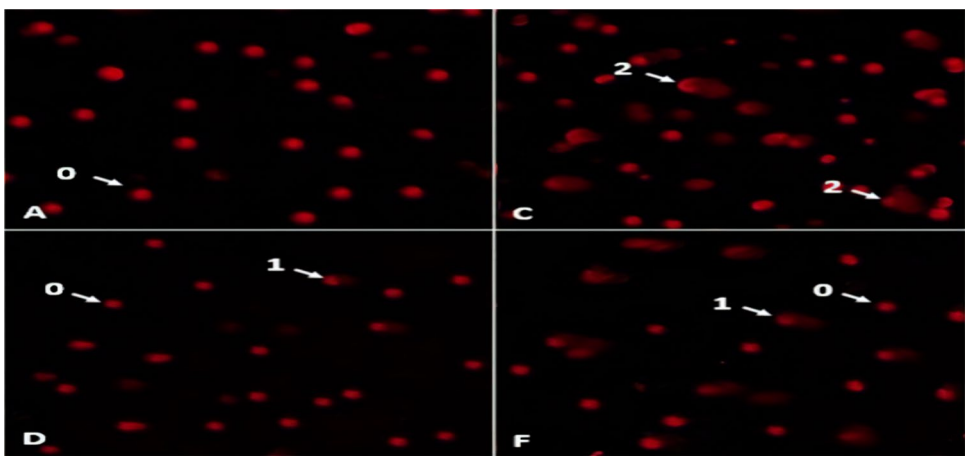

Fig. 17 **A**, **D** Fluorescence microscopy images of untreated breast cancer cells MCF-7 cells, **C**, **F** images of treated MCF-7 cells by EOs-AgNPs dependent IC_{50} concentration

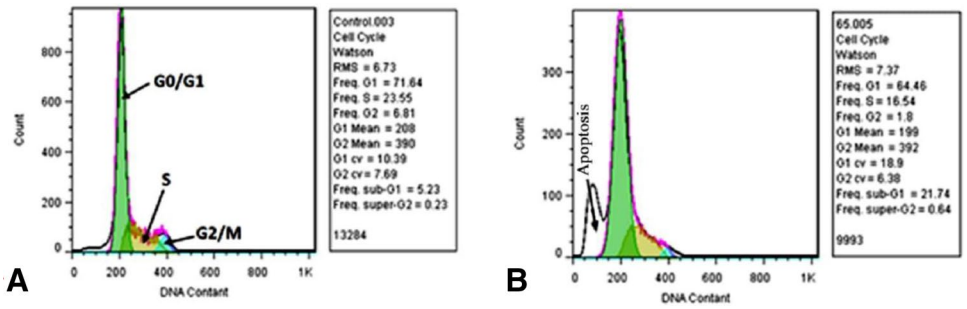

Fig. 18 **A** Cell cycle arrested technique of untreated breast cancer MCF-7 cells, **B** EOs-AgNPs suppressing breast cancer of MCF-7 cells carcinoma growth

breast cancer cells (Sathishkumar et al. 2016; Mishra et al. 2021).

Arresting cell cycle of breast carcinoma

Following 24 h treatment period, the impact of EOs-AgNPs on the course of the cell cycle was assessed based on (IC_{50}) determined. In the current study, cell cycle arrest led to a decrease in the G0/G1 population, which corresponded to an increase in the sub-G1 simultaneously augmented apoptosis index, indicating increased destruction of the MCF-7 breast cancer cell line (Fig. 18A). Consequently, cells treated with AgNPs (Fig. 18B) exhibited an increased index of the sub-G1 cell population, which led to the initiation of the genotoxic procedure. Cell cycle technique appeared the DNA content of cells treated with Ag NPs for 24 h significantly decreased, corroborating findings from other studies involving various plant substances along with organic solvents (Behboodi et al. 2019; Khader et al. 2020). According to our knowledge, no study or research is concerning the MCF-7 breast cancer activity of AgNPs synthesized by essential oils extracted from Iraqi *Jasminum sambac* leaves.

Conclusion

Essential oils serve as both reducing and capping agents. The utilization of the green technique for the synthesis of silver nanoparticles in a single step proves to be an affordable approach. This method does not require any challenging conditions, such as high temperatures, avoidance of light, or the use of additional instruments like a microwave. Moreover, it is environmentally friendly, as it employs not harmful solvents less time-consuming, and solves the problem of the differing polarities of ethanol and distilled water. Biosynthesis of EOs-AgNPs in a single step results in a greater propensity for cellular uptake. It is known that the antibacterial activity of EOs-AgNPs increases the inhibition zones of Gram-positive *S. aureus* and Gram-negative *E. coli*. In considering EOs-AgNPs as antibacterial, there are two significant considerations. Low concentrations of EOs-AgNPs specific to *S. aureus* and *E. coli* were preferred for more effectively inhibiting bacterial growth. Secondly, *regarding E. coli* resistance to AgNPs due to the LPS outer layer, the presented findings clarify the role of low concentration in obtaining highly inhibited E. coli growth. The MTT assay suggests that the created EOs-AgNPs had anticancer properties, as they inhibited the growth of MCF-7 cancer cells at an IC_{50} concentration of 260 µg/mL. In the Comet experiment, DNA damage suggested that ROS-induced DNA strand breaks may play a role, emphasized by the flow cytometry technique. On the other side, the library requires additional research into significant properties of metallic nanostructures (i.e., shape, size, hydrodynamic radii, and surface charge) associated with decreasing microbe rebellion. Especially, at this study managed forward discourage Gram-negative *E. coli*, the possibility to test created EOs-AgNPs as proposed inhibition resistance in vivo compared to the ordinary antibiotic which exposed to the resistance of bacteria.

Acknowledgements My special thanks go to the Department of Chemistry at the College of Science at the University of Basrah in Basrah, Iraq. Our work is made more accessible by it.

Funding The authors did not receive support from any organization for the submitted work.

Data availability The data that supports the findings of this study are available within the article.

Declarations

Conflict of interest The authors declare that they have no conflict of interest in the publication.

Informed consent There are no human participants involved in this work.

References

Agnihotri S, Mukherji S, Mukherji S (2014) Size-controlled silver nanoparticles synthesized over the range 5–100 nm using the same protocol and their antibacterial efficacy. Rsc Adv 4:3974–3983. https://doi.org/10.1039/C3RA44507K

Alharbi NS, Khaled JM, Alanazi K, Kadaikunnan S, Alobaidi AS (2023) Biosynthesis of silver nanoparticles (Ag-NPs) using *Senna*

alexandrina grown in Saudi Arabia and their bioactivity against multidrug-resistant pathogens and cancer cells. Saudi Pharm J 31(6):911–920. https://doi.org/10.1016/j.jsps.2023.04.015

Ali MA, Farah MA, Al-Hemaid FM, Abou-Tarboush FM, Al-Anazi KM, WabaIDUR S, Alothman Z, Lee J (2016) Assessment of biological activity and UPLC–MS based chromatographic profiling of ethanolic extract of *Ochradenus arabicus*. Saudi J Biol Sci 23(2):229–236. https://doi.org/10.1016/j.sjbs.2015.02.010

Ali N, Bilal M, Khan A, Ali F, Khan H, Khan HA, Iqbal HM (2021) Fabrication strategies for functionalized nanomaterials. Muhammad BT, Muhammad S, Abdullah AM (eds) Nanomaterials: synthesis, characterization, hazards and safety. Elsevier, Switzierland, pp 55–95. https://doi.org/10.1016/B978-0-12-823823-3.00010-0

Al-Kawmani AA, Alanazi KM, Farah MA, Ali MA, Hailan WAQ, Al-Hemaid FM (2020) Apoptosis-inducing potential of biosynthesized silver nanoparticles in breast cancer cells. J King Saud Univ Sci 32(4):2480–2488. https://doi.org/10.1016/j.jksus.2020.04.002

Al-Majeed SHA, Al-Ali ZSA, Turki AA (2023) Biomedical assessment of silver nanoparticles derived from L-aspartic acid against breast cancer cell lines and bacteria strains. BioNanoSci 13:1833–1848. https://doi.org/10.1007/s12668-023-01198-8

Alsharif SM, Salem SS, Abdel-Rahman MA, Fouda A, Eid AM, Hassan SE-D, Awad MA, Mohamed AA (2020) Multifunctional properties of spherical silver nanoparticles fabricated by different microbial taxa. Heliyon 6(5):e03943. https://doi.org/10.1016/j.heliyon.2020.e03943

Amenah SK, Al-Ali ZS (2024) Reduce graphene oxide nanosheets derived from *Iraqi rhhus* Coriaria(L.) Fruits were evaluated for their anticancer and antibacterial properties. Revista Facultad De Ciencias. https://doi.org/10.15446/rev.fac.cienc.v12n2.104545

Ammari H, Deng Y, Millien P (2016) Surface plasmon resonance of nanoparticles and applications in imaging. Arch Rational Mech Anal 220:109–153. https://doi.org/10.1007/s00205-015-0928-0

Azizi S, Ahmad M, Mahdavi M, Abdolmohammadi S (2013) Preparation, characterization, and antimicrobial activities of ZnO nanoparticles/cellulose nanocrystal nanocomposites. BioRes 8(2):1841–1851

Balasubramanian S, Kala SMJ, Pushparaj TL (2020) Biogenic synthesis of gold nanoparticles using *Jasminum auriculatum* leaf extract and their catalytic, antimicrobial and anticancer activities. J Drug Delivery Sci Technol 57:101620. https://doi.org/10.1016/j.jddst.2020.101620

Behboodi S, Baghbani-Arani F, Abdalan S, Shandiz SAS (2019) Green engineered biomolecule-capped silver nanoparticles fabricated from *Cichorium intybus* extract: in vitro assessment on apoptosis properties toward human breast cancer (MCF-7) cells. Biol Trace Elem Res 187:392–402. https://doi.org/10.1007/s12011-018-1392-0

Bhattacharjee S (2016) DLS and zeta potential–what they are and what they are not? J Control Rel 235:337–351. https://doi.org/10.1016/j.jconrel.2016.06.017

Bhavyasree P, Xavier T (2021) A critical green biosynthesis of novel CuO/C porous nanocomposite via the aqueous leaf extract of *Ficus religiosa* and their antimicrobial, antioxidant, and adsorption properties. Chem Eng J Adv 8:100152

Bidan AK, Al-Ali ZSA (2022) Biomedical evaluation of biosynthesized silver nanoparticles by *Jasminum sambac* (L.) aiton against breast cancer cell line, and both bacterial strains colonies. Int J Nanosci. https://doi.org/10.1142/S0219581X22500429

Bidan AK, Al-Ali ZSA (2023) Oleic and palmitic acids with bioderivatives essential oils synthesized of spherical gold nanoparticles and its anti-human breast carcinoma MCF-7 in vitro examination. BioNanoSci. https://doi.org/10.1007/s12668-023-01172-4

Bidan AK, Al-Ali ZSA (2024a) Assessment defeating of breast cancer MCF-7 cells, and bacterial species by spherical gold nanoparticles fabricated through reductive ability of framed bio-organic molecules. Chem Afr. https://doi.org/10.1007/s42250-024-00979-2

Bidan AK, Al-Ali ZSA (2024b) The role of biomaterial constituents of *Jasminum sambac* (L.) Aiton leaves in copper nanoparticles synthesis and evaluates their activities as anti-breast cancer and antibacterial agents. Inorg Nano Met Chem. https://doi.org/10.1080/24701556.2024.2354480

Boutinguiza M, Comesaña R, Lusquiños F, Riveiro A, Del Val J, Pou J (2015) Production of silver nanoparticles by laser ablation in open air. Appl Surf Sci 336:108–111. https://doi.org/10.1016/j.apsusc.2014.09.193

Braun NA, Sim S (2012) Jasminum sambac flower absolutes from India and China-geographic variations. Nat Prod Commun. https://doi.org/10.1177/1934578X1200700526

Bunaciu A, Udriştioiu EG, Aboul-Enein HY (2015) X-ray diffraction: instrumentation and applications. Crit Rev Anal Chem 45:289–299

Dua TK, Giri S, Nandi G, Sahu R, Shaw TK, Paul P (2023) Green synthesis of silver nanoparticles using *Eupatorium adenophorum* leaf extract: characterizations, antioxidant, antibacterial and photocatalytic activities. Chem Pap 77:2947–2956. https://doi.org/10.1007/s11696-023-02676-9

El-Hawary SS, El-Hefnawy HM, Osman SM, Mostafa ES, Mokhtar F, El-Raey M (2019) Chemical profile of two *Jasminum sambac* L.(Ait) cultivars cultivated in Egypt-their mediated silver nanoparticles synthesis and selective cytotoxicity. Int J Appl Pharm 11(6):33646. https://doi.org/10.22159/ijap.2019v11i6.33646

Farah MA, Ali MA, Chen S-M, Li Y, Al-Hemaid FM, Abou-Tarboush FM, Al-Anazi KM, Lee J (2016) Silver nanoparticles synthesized from Adenium obesum leaf extract induced DNA damage, apoptosis and autophagy via generation of reactive oxygen species. Colloids Surf B 141:158–169. https://doi.org/10.1016/j.colsurfb.2016.01.027

Fröhlich E (2012) The role of surface charge in cellular uptake and cytotoxicity of medical nanoparticles. Int J Nanomed 7:5577–5591

Gao H, Yang H, Wang C (2017) Controllable preparation and mechanism of nano-silver mediated by the microemulsion system of the clove oil. Results Phys 7:3130–3136. https://doi.org/10.1016/j.rinp.2017.08.032

Guan Z, Ying S, Ofoegbu PC, Clubb P, Rico C, He F, Hong J (2022) Green synthesis of nanoparticles: current developments and limitations. Environ Technol Innov 26:102336. https://doi.org/10.1016/j.eti.2022.102336

Gupta A, Mumtaz S, Li C-H, Hussain I, Rotello VM (2019) Combatting antibiotic-resistant bacteria using nanomaterials. Chem Soc Rev 48:415–427. https://doi.org/10.1039/C7CS00748E

He L-L, Wang X, Wu X-X, Wang Y-X, Kong Y-M, Liu B-M, Liu B (2015) Protein damage and reactive oxygen species generation induced by the synergistic effects of ultrasound and methylene blue. Spectrochim Acta A 134:361–366. https://doi.org/10.1016/j.saa.2014.06.121

Holder CF, Schaak RE (2019) Tutorial on powder X-ray diffraction for characterizing nanoscale materials. ACS Nano 13(7):7359–7365. https://doi.org/10.1021/acsnano.9b05157

Kalishwaralal K, Deepak V, Pandian SRK, Kottaisamy M, Barathmanikanth S, Kartikeyan B, Gurunathan S (2010) Biosynthesis of silver and gold nanoparticles using *Brevibacterium casei*. Colloids Surf B 77:257–262. https://doi.org/10.1016/j.colsurfb.2010.02.007

Karimi J, Mohsenzadeh S (2015) Rapid, green, and eco-friendly biosynthesis of copper nanoparticles using flower extract of Aloe vera. Synth React Inorg Met Org Nano Met Chem 45(6):895–898. https://doi.org/10.1080/15533174.2013.862644

Kennedy DC, Orts-Gil G, Lai C-H, Muller L, Haase A, Luch A, Seeberger PH (2014) Carbohydrate functionalization of silver nanoparticles modulates cytotoxicity and cellular

uptake. J Nanobiotechnol 12:1–8. https://doi.org/10.1186/s12951-014-0059-z
Khader SZA, Syed ZAS, Ganesan GM, Mahboob MR, Vetrivel M, Sankarappan M, Manickam P (2020) *Rhynchosia rufescens* AgNPs enhance cytotoxicity by ROS-mediated apoptosis in MCF-7 cell lines. Environ Sci Pollut Res 27:2155–2164. https://doi.org/10.1007/s11356-019-06479-y
Khan SA (2020) Metal nanoparticles toxicity: Role of physicochemical aspects. Muhammad RS, Muhammad I, Shafi U (ed) Metal nanoparticles for drug delivery and diagnostic applications, Elsevier, pp 1–11. https://doi.org/10.1016/B978-0-12-816960-5.00001-X
Landeros-Páramo L, Saavedra-Molina A, Gómez-Hurtado MA, Rosas G (2022) The effect of AgNPS bio-functionalization on the cytotoxicity of the yeast *Saccharomyces cerevisiae*. 3 Biotech 12:196. https://doi.org/10.1007/s13205-022-03276-2
Lava M, Muddapur UM, Basavegowda N, More SS, More VS (2021) Characterization, anticancer, antibacterial, anti-diabetic and anti-inflammatory activities of green synthesized silver nanoparticles using *Justica wynaadensis* leaves extract. Mater Today Proc 46:5942–5947. https://doi.org/10.1016/j.matpr.2020.10.048
Lee W-C, Lee B-T, Lee S, Hwang YS, Jo E, Eom I-C, Lee S-W, Kim S-O (2016) Optimisation, evaluation and application of asymmetrical flow field-flow fractionation with single particle inductively coupled plasma mass spectrometry (SP-ICP-MS) to characterise silver nanoparticles in environmental media. Microchem J 129:219–230. https://doi.org/10.1016/j.microc.2016.06.030
Logeswari P, Silambarasan S, Abraham J (2015) Synthesis of silver nanoparticles using plants extract and analysis of their antimicrobial property. J Saudi Chem Soc 19:311–317. https://doi.org/10.1016/j.jscs.2012.04.007
Maciel MVDOB, Da Rosa AA, Machado MH, Elias WC, Da Rosa CG, Teixeira GL, Noronha CM, Bertoldi FC, Nunes MR, De Armas RD (2020) Green synthesis, characteristics and antimicrobial activity of silver nanoparticles mediated by essential oils as reducing agents. Biocatal Agric Biotechnol 28:101746. https://doi.org/10.1016/j.bcab.2020.101746
Manukumar H, Umesha S, Kumar HN (2017) Promising biocidal activity of thymol loaded chitosan silver nanoparticles (TC@AgNPs) as anti-infective agents against perilous pathogens. Int J Biol Macromol 102:1257–1265. https://doi.org/10.1016/j.ijbiomac.2017.05.030
Mishra J, Kour A, Amin DS, Panda JJ (2021) Biofabricated smart-nanosilver: promising armamentarium for cancer and pathogenic diseases. Colloid Interface Sci Commun 44:100459. https://doi.org/10.1016/j.colcom.2021.100459
Morales-Lozoya V, Espinoza-Gómez H, Flores-López LZ, Sotelo-Barrera EL, Núñez-Rivera A, Cadena-Nava RD, Alonso-Nuñez G, Rivero IA (2021) Study of the effect of the different parts of *Morinda citrifolia* L(noni) on the green synthesis of silver nanoparticles and their antibacterial activity. Appl Surf Sci 537:147855. https://doi.org/10.1016/j.apsusc.2020.147855
Naseer A, Ali A, Ali S, Mahmood A, Kusuma H, Nazir A, Yaseen M, Khan M, Ghaffar A, Abbas M (2020) Biogenic and eco-benign synthesis of platinum nanoparticles (Pt NPs) using plants aqueous extracts and biological derivatives: environmental, biological and catalytic applications. J Mater Res Technol 9:9093–9107. https://doi.org/10.1016/j.jmrt.2020.06.013
Nguyen T, Huynh T, Dang C-H, Mai D-T, Nguyen T, Nguyen D-T, Dang V-S, Nguyen T-D, Nguyen T-D (2020) Novel biogenic silver nanoparticles used for antibacterial effect and catalytic degradation of contaminants. Res Chem Intermed 46:1975–1990. https://doi.org/10.1007/s11164-019-04075-w
Piao MJ, Kang KA, Lee IK, Kim HS, Kim S, Choi JY, Choi J, Hyun JW (2011) Silver nanoparticles induce oxidative cell damage in human liver cells through inhibition of reduced glutathione and induction of mitochondria-involved apoptosis. Toxicol Lett 201:92–100. https://doi.org/10.1016/j.toxlet.2010.12.010
Pretsch E, Buhlmann P, Affolter C, Pretsch E, Bhuhlmann P, Affolter C (2020) Structure determination of organic compounds. Springer, Berlin. https://doi.org/10.1007/978-3-662-62439-5
Princy SSJ, Hentry C, Alodaini HA, Hatamleh AA, Arokiyaraj S, Bindhu M (2023) Hibiscus cannabinus seeds assisted spherical silver nanoparticles and its antibacterial and photocatalytic applications. Chem Phys Impact 6:100192. https://doi.org/10.1016/j.chphi.2023.100192
Pryshchepa O, Pomastowski P, Buszewski B (2020) Silver nanoparticles: synthesis, investigation techniques, and properties. Adv Colloid Interface Sci 284:102246. https://doi.org/10.1016/j.cis.2020.102246
Rogers B, Adams J, Pennathur S (2007) Nanotechnology: understanding small systems. CRC Press, London. https://doi.org/10.1201/9781439896716
Sathishkumar P, Vennila K, Jayakumar R, Yusoff A, Hadibarata PT (2016) Phyto-synthesis of silver nanoparticle using *Alternanthera tenella* leaf extract: An effective inhibitor for the migration of human breast adenocarcinoma (MCF-7) cells. Bioprocess Biosyst Eng 39:651–659. https://doi.org/10.1007/s00449-016-1546-4
Selvan DA, Mahendiran D, Kumar RS, Rahiman AK (2018) Garlic, green tea and turmeric extracts-mediated green synthesis of silver nanoparticles: phytochemical, antioxidant and in vitro cytotoxicity studies. J Photochem Photobiol B 180:243–252. https://doi.org/10.1016/j.jphotobiol.2018.02.014
Shankar SS, Rai A, Ahmad A, Sastry M (2004) Rapid synthesis of Au, Ag, and bimetallic Au core–Ag shell nanoparticles using Neem (*Azadirachta indica*) leaf broth. J Colloid Interface Sci 275:496–502. https://doi.org/10.1016/j.jcis.2004.03.003
Sheny D, Mathew J, Philip D (2012) Synthesis characterization and catalytic action of hexagonal gold nanoparticles using essential oils extracted from *Anacardium occidentale*. Spectrochim Acta A 97:306–310. https://doi.org/10.1016/j.saa.2012.06.009
Si S, Mandal TK (2007) Tryptophan-based peptides to synthesize gold and silver nanoparticles: a mechanistic and kinetic study. Chem Eur J 13:3160–3168. https://doi.org/10.1002/chem.200601492
Singh NP, Mccoy MT, Tice RR, Schneider EL (1988) A simple technique for quantitation of low levels of DNA damage in individual cells. Exp Cell Res 175:184–191. https://doi.org/10.1016/0014-4827(88)90265-0
Singh AK, Talat M, Singh D, Srivastava O (2010) Biosynthesis of gold and silver nanoparticles by natural precursor clove and their functionalization with amine group. J Nanopart Res 12:1667–1675. https://doi.org/10.1007/s11051-009-9835-3
Tahir MB (2018) Construction of MoS2/CND-WO3 ternary composite for photocatalytic hydrogen evolution. J Inorg Organomet Polym Mater 28:2160–2168. https://doi.org/10.1007/s10904-018-0867-y
Tanaka K (1999) Nanotechnology towards the 21st century. Thin Solid Films 341:120–125. https://doi.org/10.1016/S0040-6090(98)01508-9
Tshikantwa TS, Ullah MW, He F, Yang G (2018) Current trends and potential applications of microbial interactions for human welfare. Front Microbiol 9:1156. https://doi.org/10.3389/fmicb.2018.01156
Verma C, Ebenso EE, Quraishi M (2019) Transition metal nanoparticles in ionic liquids: synthesis and stabilization. J Mol Liq 276:826–849. https://doi.org/10.1016/j.molliq.2018.12.063
Vilas V, Philip D, Mathew J (2014) Catalytically and biologically active silver nanoparticles synthesized using essential oil. Spectrochim Acta A 132:743–750. https://doi.org/10.1016/j.saa.2014.05.046
Vilas V, Philip D, Mathew J (2016) Essential oil mediated synthesis of silver nanocrystals for environmental, anti-microbial and antioxidant applications. Mater Sci Eng C 61:429–436. https://doi.org/10.1016/j.msec.2015.12.083

Wang R, Xing Z, Wang M, Gui Y, Yang M (2020) Biosynthesis of AgNPs and their synergistic effect in combination with ultrasound waves on breast cancer cells. J Drug Deliv Sci Technol 60:101975. https://doi.org/10.1016/j.jddst.2020.101975

Wiersema J, Taxonomy G (2019) US national plant germplasm system. Checklist Dataset. https://doi.org/10.15468/ao14pp

Wu Q, Miao W-S, Gao H-J, Hui D (2020) Mechanical properties of nanomaterials: a review. Nanotechnol Rev 9:259–273. https://doi.org/10.1515/ntrev-2020-0021

Yeh Y-C, Creran B, Rotello VM (2012) Gold nanoparticles: preparation, properties, and applications in bionanotechnology. Nanoscale 4:1871–1880. https://doi.org/10.1039/C1NR11188D